LRP 519/95 June 1995

OVERVIEW OF ALFVEN EIGENMODE EXPERIMENTS IN JET

A. Fasoli, J.B. Lister, S. Sharapov, S. Ali-Arshad,
G. Bosia, D. Borba, D.J. Campbell, N. Deliyanakis,
J.A. Dobbing, C. Gormezano, H.A. Holties,
G.T.A. Huysmans, J. Jacquinot, A. Jaun,
W. Kerner, P. Lavanchy, J.-M. Moret, L. Porte,
A. Santagiustina, L. Villard

Paper presented at the
4th IAEA Technical Committee Meeting
on Alpha Particles in Fusion Research
held at Princeton Plasma Physics Laboratory
Princeton, U.S.A., April 25-28, 1995

Overview of Alfvén Eigenmode Experiments in JET

A.Fasoli[1], J.B.Lister[1], S.Sharapov, S.Ali-Arshad, G.Bosia, D.Borba, D.J.Campbell, N.Deliyanakis, J.A.Dobbing, C.Gormezano, H.A.Holties[2], G.T.A.Huysmans, J.Jacquinot, A.Jaun[1], W.Kerner, P.Lavanchy[1], J.-M.Moret[1], L.Porte, A.Santagiustina, L.Villard[1]

JET Joint Undertaking, Abingdon, Oxon OX14 3EA, UK.

[1]Centre de Recherches en Physique des Plasmas, Association EURATOM-Confédération Suisse, Ecole Polytechnique Fédérale de Lausanne, 1015 Lausanne, Switzerland.
[2]FOM Institute for Plasma Physics, Rijnhuizen, Nieuwegein, Netherlands.

Abstract

Results from the first experiments to drive Alfven Eigenmodes (AE) with antennas external to a tokamak plasma are presented. In Ohmically heated plasma discharges, direct experimental measurements of the damping of Toroidicity induced AE (TAE) have allowed an identification of different regimes corresponding to different dominant TAE absorption mechanisms with a wide range of damping rates, $10^{-3} \leq \gamma/\omega \leq 10^{-1}$. In plasmas heated by ion cyclotron resonance heating, neutral beam injection heating, lower hybrid heating and high plasma current ohmic heating, a new class of weakly damped Alfvén eigenmodes, the Kinetic Alfvén Eigenmodes, predicted in theoretical models which include finite Larmor radius and finite parallel electric field effects, has been identified experimentally.

Overview of Alfvén Eigenmode Experiments in JET

A.Fasoli[1], J.B.Lister[1], S.Sharapov, S.Ali-Arshad, G.Bosia, D.Borba, D.J.Campbell, N.Deliyanakis, J.A.Dobbing, C.Gormezano, H.A.Holties[2], G.T.A.Huysmans, J.Jacquinot, A.Jaun[1], W.Kerner, P.Lavanchy[1], J.-M.Moret[1], L.Porte, A.Santagiustina, L.Villard[1]

JET Joint Undertaking, Abingdon, Oxon OX14 3EA, UK.

[1]Centre de Recherches en Physique des Plasmas, Association EURATOM-Confédération Suisse, Ecole Polytechnique Fédérale de Lausanne, 1015 Lausanne, Switzerland.

[2]FOM Institute for Plasma Physics, Rijnhuizen, Nieuwegein, Netherlands.

1. Introduction and Motivation

Weakly damped Alfvén Eigenmodes, AE, which exist within the shear Alfvén spectrum in toroidal devices [1,2], are recognised as important for confinement of alpha particles created by fusion reactions in D-T magnetically confined plasmas. Resonant wave-particle processes between AE and fast ions can both drive the modes unstable and produce modifications to the particle orbits [3]. Above a certain threshold amplitude, AE can induce stochasticity in the particle trajectories and consequently anomalous phase space particle transport and losses [4]. By coupling to other loss mechanisms, such as magnetic ripple effects, wall damage can also be caused. During slowing-down, a significant fraction of the alpha particle population created by fusion reactions will satisfy the resonance condition $v \sim v_{Alfvén}$, where $v_{Alfvén}=B_{tor}/(\mu_0\rho)^{1/2}$ is the mode phase velocity, ρ is the mass density and B_{tor} the toroidal magnetic field. In ignited plasmas the slowing down alpha population provides the major source of heating, with large amounts of energy and steep pressure gradients constituting a source for the excitation of AE. Even a fractional loss of alpha particles can produce deleterious consequences on the first wall as well as on heating deposition profiles [5].

In order to assess the linear stability of Alfvén eigenmodes, both driving and damping effects must be investigated. The theoretical evaluation of these terms is made extremely delicate by the concurrence of MHD and kinetic effects. The predictions of the damping rates

vary by more than one order of magnitude, according to the *a priori* assumptions characterising different models.

Existing experimental results on the role of Alfvén eigenmodes in affecting transport in present tokamak plasmas also vary considerably. AE activity driven by resonant energetic particles produced by Neutral Beam Injection (NBI) and Ion Cyclotron Resonance Heating (ICRH), has been reported for different tokamak experiments [6-10]. Fast particle losses together with a sudden reduction of the neutron production rate have been observed at the same time as bursts of Toroidicity induced AE (TAE) [5]. In similar experiments in deuterium-tritium plasmas, no increase in the lost alpha flux was observed in the presence of TAE activity [11]. Such passive studies, although providing frequency and mode spectra as well as some information on the instability thresholds and saturation levels, can not provide quantitative estimates of the damping and driving of the Alfvén eigenmodes. In addition to the balance between driving and damping terms, determining the mode stability, it is necessary to evaluate the frequency spectra and spatial distributions in order to assess the effect on particle orbits for cases in which the modes cannot be stabilised.

A new active diagnostic system, combining excitation by external antennas with coherent detection of various probing signals at the plasma edge and in the core, has been developed to perform these studies on the JET tokamak independently of the intrinsic driving effects due to resonant fast particles [12]. This method has the major advantage of providing a direct measurement of the damping rates of the Alfvén eigenmodes, leading to investigations into the relevant absorption mechanisms in various plasma conditions. Similar experiments had previously only been carried out in the discrete Alfvén wave range of frequencies on the TCA, PETULA and TEXTOR tokamaks [13-15]. In the first part of this paper we present the experimental arrangement and method, results on the identification of the eigenmode dispersion relation and the first measurements of the damping rate for Toroidicity induced Alfvén Eigenmodes in relatively cold, ohmic JET plasmas.

In the second part of the paper we report on the investigation as to how the AE spectral features are modified in additionally heated plasmas. Theoretically, the description of TAE in hot plasmas has recently been refined by including kinetic effects in the models, producing two new results: a novel absorption mechanism for TAE, referred to as radiative damping, and the appearance, in the frequency range associated with the TAE, of new families of weakly damped discrete modes, the Kinetic Toroidal Alfvén Eigenmodes (KTAE) [16-19]. As KTAE are intrinsically exempt from radiative damping, with continuum damping

replaced by mode coupling between KTAE with frequencies above the TAE gaps [17,18], their total damping rates and instability thresholds can be lower than those of the TAE. Several KTAE may be associated with every TAE gap. Thus, for a given plasma equilibrium, the number of KTAE that can be simultaneously excited can be much larger than that of TAE and the relative stochastic threshold amplitude could be reduced significantly [20, 21]. Different plasma heating methods were applied, including Ion Cyclotron Resonance Heating (ICRH), Neutral Beam Injection (NBI), Lower Hybrid Heating (LHH) and high current ohmic heating, in order to produce larger ion Larmor radii, higher electron and ion temperatures and larger electron to ion temperature ratios with respect to the cold plasma case, in which the Alfvén eigenmode spectra are characterised by a very small number of modes in the TAE gap. These conditions led to the first experimental observation of multiple peak structures in the TAE frequency region.

2. Experimental method

2.1 External antenna excitation

The JET saddle coils, four above and four below the plasma, situated 90^0 apart toroidally and covering poloidal and toroidal extensions of about 60^0 and 90^0, have been used as external antennas to excite the Alfvén eigenmodes. The AE exciter has been developed to cover most of the AE frequency range, including pressure and ellipticity induced eigenmodes, from 30 to 500 kHz. The launching apparatus encompasses a remotely controllable function generator, a 3 kW broad band power amplifier, an impedance matching network, a power distribution and an isolation unit. The apparatus is connected to the saddle coils via a low loss, 80 m, 50 ohm transmission line. A general lay-out of the AE exciter is reported in Fig.1. The power distribution unit connects the amplifier output to the active antennas (1, 2 or 4 saddle coils), allowing different combinations of antenna phasing that can preferentially excite specific low toroidal mode numbers. Electrical insulation up to 10 kV between the saddle coils and the launching apparatus is guaranteed by a set of ferrite core transformers. Input current and voltage are measured at the distribution unit, whilst the voltage measurements on both the active and passive saddle coils are taken at the isolation unit. Currents on the saddle coils are measured at the end of the transmission line, at the machine transformer limb. Maximum currents and voltages induced in the saddle coils by the AE exciter in the present configuration are of the order of 30 A and 500 V, respectively. The resistive power radiated by the saddle coils does not exceed 300 W. The magnetic perturbations in the plasma core

are such that $\delta B/B<10^{-5}$. As a result, the excited AE amplitudes are not expected to perturb the plasma significantly, e.g. in form of enhanced transport of energetic particles.

2.2 Diagnostic method

The excitation frequency is swept across the shear Alfvén gap regions, where AE are expected. The plasma response is determined in terms of driven oscillating quantities such as magnetic fields and densities. The driven component is extracted from background noise in various diagnostic signals using a set of synchronous detectors which provide the in phase and quadrature components of the signals, i.e. their real and imaginary parts in a complex representation. Band pass filters from 20 kHz to 500 kHz are used to feed the signals to the synchronous detectors. The output bandwidth of the coherent detection system is about 500 Hz. Signals are then digitised at a sampling rate of 1 kHz. Different diagnostic channels are equipped with such detection. The voltage and current of the excited saddle coils provide the antenna impedance. The induced voltage on the passive saddle coils and the fast magnetic pick-up coils measure the perturbation of the radial and poloidal B-fields, allowing a mode analysis both in the poloidal and toroidal conjugate planes. Other non-magnetic diagnostics, such as heterodyne ECE and microwave reflectometry, are coupled to the synchronous detectors to obtain information on the radial structure of the excited global mode.

The time and frequency resolution of the frequency and damping measurements are interdependent and linked to the frequency sweep rate. The latter is limited on the upper side by the intrinsic plasma noise level and the integration time needed to extract the driven signal in the synchronous detection chain, and on the lower side by the characteristic time scale for variations of the plasma parameters which define the resonant frequency. Typical figures for the time and frequency resolutions in the plasmas studied are 100-500 ms and less than 1 kHz respectively, with sweep rates of the order of 200 kHz/s.

3. Data analysis and representation

The transfer function between the driving current and any particular diagnostic signal can be directly derived from the raw data by normalising that signal response to the antenna current. The presence of an Alfvén eigenmode manifests itself as a resonance in this transfer function, H, which can be represented in terms of complex conjugate poles, p_k and p_k^*, and residues, r_k and r_k^*

$$H(\omega,x)=\sum_{k=1}^{N}\frac{1}{2}\left(\frac{r_k(x)}{i\omega-p_k}+\frac{r_k^{*}(x)}{i\omega-p_k^{*}}\right)+D(\omega,x)=\frac{B(\omega,x)}{A(i\omega)}$$

Here N is the number of resonances in the measurement range, ω is the driving frequency and x is the measurement position. For the k^{th} resonance, $p_k=i\omega_{0k}+\gamma_k$ defines a pole which is common to all diagnostic signals, with ω_{0k} being the resonant (real) frequency and γ_k the damping rate. Since the signals may contain a direct, non-resonant coupling with the antenna, an additional scalar quantity D is added to the first order resonance terms.

The data from a complete set of diagnostic signals are analysed by simultaneously fitting the above expression to all of the signals, with a single denominator A which determines the resonance characteristics and separate numerators B [22]. By imposing a pole common to all transfer functions, the statistical errors in the evaluation of the poles are reduced and the estimates of the residues are then reliable even for noisy signals. The fitted pole provides two pieces of information. Its imaginary part gives the frequency of the mode, $f_{obs}=\omega_{0k}/2\pi$. Its real part, in the case of stable modes, is the algebraic difference between the damping rate and the growth rate: $\gamma=\gamma_{damping}-\gamma_{drive}$. In particular, if no fast particle driving terms are present in the plasma, $\gamma_{drive}=0$ and γ corresponds directly to the damping rate of the mode. For those diagnostic signals which are space-resolved measurements of the vacuum wave field, the residues correspond directly to the wave amplitude as a function of space, i.e. to the single mode structure.

4. Excitation and identification of TAE and EAE

In this section, we focus our attention on active measurements performed in the ohmic phase of JET deuterium discharges on relatively cold plasmas. Several global eigenmodes have been clearly observed in the range 60-300 kHz in different plasma conditions. An example of a resonance detected on one of the magnetic field probes is shown in Fig. 2. The signal amplitude, normalised to the complex amplitude of the current driven in the active antenna, describes a circle in the complex plane as the frequency is swept across the resonance. The maximum value of the oscillating magnetic field measured by the coil is of the order of 10^{-7} T for driving currents of the order of 5A in each antenna. This resonance behaviour was seen simultaneously on all of the magnetic field pick-up coils, as well as on the unexcited saddle coils. With numerator and denominator chosen of order 5 and 2, the fit provides an accurate value for the eigenmode frequency, f_{obs}=144.2+-0.1 kHz, and for its

damping rate $\gamma/2\pi$=1400+-100 s^{-1}, corresponding to a relatively large resonance quality factor, $Q=\omega/\gamma\sim125$, or equivalently, to a relatively weak damping, $\gamma/\omega\sim0.8\%$.

The 'Alfvén' character of the measured resonances was verified from the dependence of their frequency on the magnetic field, plasma density and current. Figure 3 shows an example of a discharge in which the toroidal magnetic field was varied from 2.2 to 3.0 T. The measured frequency agrees well with the value corresponding to the centre of the toroidicity induced gap, $f^0_{TAE}\cong v_{Alfvén}/(4\pi qR_0)$, where q is the safety factor and R_0 is the tokamak major radius. Here f^0_{TAE} is evaluated assuming q=1.5, corresponding to the most effectively antenna driven TAE mode [23,24], and using the line-averaged plasma density ($\bar{n}_e$) for calculating $v_{Alfvén}$. The value of γ/ω remained roughly constant at $\gamma/\omega\sim1\%$. In other discharges the plasma density was varied. The mode frequency always followed f^0_{TAE}, with an inverse dependence on the square root of the density. These observations clearly demonstrate that the driven resonances are Toroidicity induced Alfvén Eigenmodes.

The reconstruction of the TAE mode structure in the poloidal and toroidal directions is shown in Fig. 4, for a discharge with two upper saddle coils driven in phase, situated 180^0 apart toroidally, providing mostly |n|=2 excitation. The phase of the residue of the response of the magnetic probes has a clear |n|=2 standing wave structure. The n=+2 and n=-2 components are excited with identical amplitudes, the toroidal symmetry being maintained both by the excitation and by the plasma itself in the absence of significant toroidal rotation. The use of the heterodyne ECE radiometer allowed in the case of relatively large driven TAE amplitudes to reconstruct the radial dependence of the perturbed magnetic field, with the assumption that no electron temperature fluctuations are associated with the TAE. The modes appeared to be localised at the gaps corresponding to the poloidal and toroidal mode numbers imposed and measured, in agreement with the numerical reconstruction of the eigenfunction for the corresponding plasma equilibrium profiles [23,24].

By extending the measurement frequency range well above the TAE gaps, a number of global modes with spatial distributions and damping rates similar to the TAE case were driven and detected. In the example shown in Fig. 5, the mode frequencies followed the $2f_{TAE}^0$ curve. These modes were thereby identified as Ellipticity Induced AE (EAE), of which the reported results constitute the first unambiguous observation.

5. Damping of TAE

Several possible damping mechanisms for TAE/EAE modes have been proposed theoretically. Firstly, *continuum damping* occurs when the eigenmode frequency intersects a shear Alfvén wave continuum at a resonant layer within the plasma. The damping by that continuum is independent of the details of the absorption mechanisms for the continuum itself but is very sensitive to the profiles q(r) and ρ(r), where r is the minor radius of the magnetic surfaces on the tokamak mid-plane. Specifically, as the gaps are centred at the local value of f^0_{TAE}, continuum damping is linked to the radial dependence of the quantity $g(r)=1/(q(r)\rho(r)^{1/2})$. If g(r) is approximately constant, the gaps are aligned and the continuum damping should be minimised. If g(r) varies strongly with r, continuum damping should become dominant and lead to large damping rates, γ/ω~5-10% [25,26]. Secondly, in the absence of strong continuum damping, several kinetic effects may become important. *Landau damping* effects are mainly due to the mode interaction with bulk ions and electrons, when $v_{th||} \sim v_{Alfvén}$ or $v_{th||} \sim v_{Alfvén}/3$. Ion Landau damping scales as $\gamma_i/\omega \propto \beta_i^{-3/2} \exp(-1/(9\beta_i))$ [27], $\beta_j = n_j T_j/(B_{tor}^2/(2\mu_0))$ being the ratio between the pressure of the species j (j=i, e) and the magnetic field pressure. γ_i is negligibly small for the ohmic discharges considered, whereas for these relatively cold and dense plasmas, $v_{the||} \sim v_{Alfvén}$ and thus electron Landau effects can contribute significantly to the damping, $\gamma_e/\omega \propto \beta_e v_{Alfvén}/v_{the||}$ [3]. Damping can also be produced by *trapped electron collisional absorption*, occurring during the transition from trapped to passing orbits, caused by collisional pitch-angle scattering, and yielding $\gamma_e^t/\omega \propto (\nu_e/\omega)^{1/2} (\beta_e q^2 + 0.1(\rho_s/\Delta_{TAE})^2)$ [28,29]. Here $\nu_e \sim n_e/T_e^{3/2}$ is the electron collision frequency, $\rho_s^2 = 2T_e/m_i\omega_{ci}^2$ and $\Delta_{TAE}^2 = \pi^2/64\ (r\varepsilon/m)^2$, with ω_{ci} being the ion cyclotron angular frequency, ε the tokamak inverse aspect ratio and m the poloidal mode number. Finally, a contribution to the Alfvén eigenmode absorption can come from *radiative damping* [30], which is a finite Larmor orbit effect of the bulk ions and leads to $\gamma_R/\omega \propto s^2 \exp(-f(s,\varepsilon)/\rho_i m)$, where f is a function of the magnetic shear s ($s=r/q\ dq/dr$) and the inverse aspect ratio, and ρ_i is the ion Larmor radius.

Greatly differing damping rates were measured in two similar discharges with different g(r). Figure 6 shows the radial dependence of g(r) obtained from the reconstructed equilibrium and the density profiles, together with the two measured eigenmodes and their damping rates. When there was a strong radial dependence of g(r), Fig. 6 curve (a), the gaps were not aligned through the continuum structure and strong damping occurred with $\gamma/\omega \sim$ 5%, in agreement with prior theoretical estimates of continuum damping [26]. The g(r)

profile in Fig. 6 curve (b) was flatter and led to a more 'open' gap structure and therefore to a much less effective continuum damping. The absorption mechanism in this case has to be sought in the kinetic interactions.

Damping rates were measured in a wide variety of conditions, in ohmically heated plasmas with 1 MA$<I_p<$3 MA, 1x10^{19} m$^{-3}<\bar{n}_e<$5x10^{19} m^{-3} and 1 T$<B_{tor}<$3.5 T. The results with both odd and even low-n excitation span several orders of magnitude, from $\gamma/\omega<0.1\%$ to $\gamma/\omega>10\%$, suggesting that different absorption mechanisms dominate according to the configuration of each specific shot. This extreme sensitivity of the damping rates of the TAE to the details of the plasma equilibrium profiles make comparisons with theoretical predictions very difficult. Even in the case of flat g(r) profiles, the measured damping appears to be at least a factor of two larger than that calculated by local models considering electron Landau and electron collisional damping in the particular case of low mode numbers. Contributions from either continuum damping at the plasma edge or by radiative damping in the core must therefore be significant and have to be accounted for.

6. Observation of multiple kinetic Alfvén eigenmodes

In additionally heated JET plasmas, characterised by larger ion Larmor radii, higher electron and ion temperatures and larger electron to ion temperature ratios with respect to the cases reported above, the AE spectral features were observed to be modified significantly. For these specific experiments two of the four lower JET saddle coils were used as external antennas in an $|n|=2$ configuration to excite modes in the frequency range 60 - 300 kHz. Different plasma heating methods were applied, including Ion Cyclotron Resonance Heating (ICRH), Neutral Beam Injection (NBI), Lower Hybrid Heating (LHH) and high current ohmic heating.

The first evidence for transitions in AE spectral features when ion and electron temperatures were increased was obtained in high current ($I_p > 3$ MA), ohmically heated plasmas. The amplitude of driven poloidal field oscillations reported in Fig. 7 shows that the single peak TAE resonance observed for low values of the plasma current is transformed, later in the same discharge, into a multiple peak structure at higher plasma current, corresponding to a hotter plasma. Each individual peak corresponds to a plasma resonance, narrower than the single TAE, characterised by a smaller value of the damping rate. As these modes are externally driven with a dominant $|n|=2$ component and the plasma toroidal rotation is negligible in JET ohmic plasmas, they cannot correspond to Doppler shifted peaks

of different n [31]. The extremely low excitation levels used and the linear dependence of the mode amplitude on the antenna current exclude non-linear antenna effects as the origin of these multiple peaks.

The most likely interpretation of these new observations in light of current theories can be found in terms of modifications of the Alfvén spectrum due to finite Larmor radius effects and to a finite wave electric field parallel to the static magnetic field. Analytical models for hot plasmas predict that several weakly damped discrete modes with regularly spaced frequencies exist inside a potential well formed above the gap, analogous to a quantum harmonic oscillator [16-19]. The occurrence of these kinetic effects is regulated by the non-ideal parameter $\lambda = 4\ m\ s\ /(r_m\ \varepsilon^{3/2})\ \rho_i\ (3/4 + T_e/T_i)^{1/2}$, where ρ_i is the ion Larmor radius, s is the local magnetic shear, $s= r/q\ dq/dr$, m the poloidal mode number and $\varepsilon \approx 2.5\ r_m/R$ with R being the tokamak major radius. λ needs to be calculated at the gap surface r_m, defined for the (m, n) mode as the location where the safety factor q is $q(r_m)=(m+1/2)/n$. Although the lack of reliable measurements of the magnetic shear prevents a systematic comparison of different plasma equilibria, qualitative indications can be obtained from relative changes of λ for similar plasma configurations. When $\lambda > \gamma/(\omega\ \varepsilon)$, kinetic effects compete with the toroidicity effects in the gap region and produce the transition from a 'cold' TAE predicted by ideal MHD models to multiple KTAE. Similarly, these kinetic effects are expected to affect the AE spectrum in the region of the ellipticity induced gap and to generate series of Kinetic Ellipticity induced Alfvén Eigenmodes, KEAE.

To confirm that it is these kinetic effects which produce the observed spectrum, we returned to equilibria which previously yielded a simple TAE and increased the temperature and hence the lambda parameter by means of additional heating. The combination of LHH and moderate ICRH in an electron or minority heating scheme constitutes an ideal scenario as T_e, T_i and T_e/T_i are raised, maximising the value of lambda while minimising AE kinetic damping without producing significant resonant fast particle populations. The latter might provide an additional driving source for AE, confusing the interpretation of the antenna-driven spectra. Figure 8 shows the spectrum of the driven magnetic and density perturbations under these conditions. Multiple resonances characterised by the same toroidal mode number appear at frequencies above the centre of the TAE gap estimated for q=1.5. This first observation of driven density perturbations in the plasma core (r/a~0.5), linked to a finite oscillating parallel electric field, emphasises the non-ideal MHD character of these modes.

Comparable spectra in the TAE/EAE gap frequency range, with similar peak frequency spacing, resonance width and mode numbers, have been observed during discharges in which other additional heating methods were applied. Multiple peaks were observed with only LHH, on both magnetic and density fluctuation measurements. The absence of resonant fast particles and of plasma rotation, together with the observed central LHH power deposition profiles, guarantee clear, Doppler-free AE signals without significant distortion of the AE gap structure. In this case the non-ideal parameter lambda is enhanced mainly through an increase in the electron to ion temperature ratio (T_e/T_i ~2-3). A series of AE resonances around the TAE gap was also seen on the magnetic signals during NBI heating, despite some interpretative difficulties raised by sheared plasma rotation and the presence of resonant particles with a high beam energy, ~140 keV. ICRH heated plasmas in a hydrogen minority scenario for electron heating again showed multiple AE in the region of the TAE gap. Relatively high magnetic field ($B \geq 2.8$ T) and intermediate power levels ($P < 6$ MW) allowed us to exclude significant effects of highly energetic trapped particles, as in the LHH case. Finally, multiple peak structures were seen during current ramp-down experiments, corresponding to sudden variations in the internal plasma inductance and presumably to rapid changes in the magnetic shear. In this case the driven perturbations appeared mainly on the reflectometer signals from the plasma core and were characterised by extremely low damping rates for the individual peaks, $\gamma/\omega < 10^{-4}$.

The very low damping rates observed for the driven KTAE/KEAE suggest that wave-particle destabilisation by a significant population of resonant particles should be easier than for TAE/EAE. By using the synchronous detection chain in a passive mode, with the reference frequency still being swept, but with no current driven in the saddle coils, it was possible to detect eigenmodes driven unstable by resonant fast particles. Multiple peaks with $f > f_{TAE}^0$ were indeed observed in these passive measurements, shown in Fig. 9 for ~7 MW of ICRH combined with ~4 MW of NBI.

In all the cases reported, the observed multiple peak structures associated with the driven AE were characterised by the simultaneous presence of several, at least 5, resonances with regular frequency spacing. An example of the peak frequency distribution for eigenmodes driven during some additionally heated JET discharges is shown in Fig. 10. The peak spacing remained similar for consecutive sweeps when the plasma conditions were maintained approximately stationary. A direct dependence of the observed frequency

distribution upon the sweep rate was excluded experimentally. The damping rates were in most cases significantly lower than for the corresponding single 'cold' TAE. Upper limits for γ/ω could be established experimentally and were in the range 10^{-3} - 10^{-4}, with no systematic variation in the damping for different peaks documented to date. In many cases each peak appeared to consist of several finer components, preventing reliable absolute estimates of the mode damping rate.

7. Numerical modelling of kinetic AE

Two complementary numerical tools, the full wave code PENN [32] and the resistive MHD code CASTOR [33], were used to study the AE spectra and specifically to calculate the linear plasma response to external driving currents in the saddle coils in axisymmetric toroidal geometry and for realistic plasma equilibria corresponding to multiple gaps. Hot plasma regimes could be investigated as both models include kinetic effects, via an expansion to second order in the ion Larmor radius in PENN [34] and via the introduction of a complex resistivity term in CASTOR [35, 36].

The results of the two codes for the conditions of the experimental results reported in Fig. 8 and for the corresponding JET equilibrium are shown in Fig. 11. At the top we see the continuum structure reconstructed by CASTOR (a), along with the eigenfrequencies of the KTAE associated with one of the TAE gaps (b), at r/a~0.5. These are characterised by a regular spacing (c), in agreement with the experimental observations. At the bottom of Fig. 11 we show the antenna loading as a function of frequency calculated by CASTOR (d) and PENN (e). Both curves indicate the presence of multiple peaks, corresponding to multiple plasma resonances, with frequencies and spacing similar to the experimental observations. Due to the plasma radial profiles, the frequency ranges of the TAE gap and the EAE gap can overlap (Fig. 5(a)). An identification of the origin of the different peaks therefore needs a reconstruction of the radial structure of the eigenfunctions. For the case of Figs. 8 and 11 the CASTOR results suggest that the externally driven modes, in the range 245 - 265 kHz, exist above the TAE gap at r/a ~ 0.5 (see Fig. 5 (b) and (c)), whereas the PENN code indicates that most peaks are associated with modes localised within the EAE gap at the plasma edge, at r/a ~ 0.9. In addition to these kinetic modes labelled on the graph with their radial mode numbers, CASTOR and PENN obtain peaks in the spectrum of the antenna loading at ~210 kHz and ~240 kHz, respectively. The former is attributed to the KTAE family associated with the neighbouring TAE gap, at r/a ~ 0.75, whilst the latter corresponds in PENN to a

mode within the TAE gap at r/a ~ 0.8. The relative coupling to the modes corresponding to the TAE or EAE gaps is found in both models to depend strongly on the details of the plasma density and safety factor profiles.

8. Discussion and Conclusions

The combination of external excitation using the JET saddle coils as antennas and synchronous detection of the diagnostic response forms the basis of the new active diagnostic for Alfvén eigenmodes on JET. The successful implementation of this diagnostic method has allowed us to drive Toroidicity induced Alfvén Eigenmodes in linearly stable conditions and to identify them by their frequency dependence on the density and the toroidal magnetic field. Control of the antenna phasing together with space resolved magnetic wave field measurements has allowed both the selection and the identification of the driven mode structure, within the range of toroidal mode numbers, $|n| < 4$, that can be driven in the plasma by the saddle coil system. The damping rates of the TAE have been experimentally measured for the first time. The large range of the measured values of γ/ω in ohmically heated discharges, due to the effect of different absorption mechanisms and specifically to continuum damping in the plasma core and at the edge, indicates the capability of the diagnostic method and emphasises the extreme sensitivity of the TAE damping to the details of the plasma equilibrium which might limit comparisons with theoretical predictions.

Under experimental conditions which correspond to the predicted departure from ideal MHD behaviour due to kinetic effects, including increased electron and ion temperatures, ion Larmor radius, electron to ion temperature ratio and changes to the magnetic shear, multiple structures of Alfvén eigenmodes have been excited and detected in the TAE gap frequency range. These modes appear to be associated with kinetic modifications of the Alfvén wave spectrum and to belong to the general class of kinetic Alfvén eigenmodes. Contrary to the cold TAE case, in which no density oscillations were observed, kinetic AE have been observed on the reflectometer diagnostic signals as well as on the magnetic probes.

In general, the reported experimental results show that multiple, very weakly damped eigenmodes can exist in the TAE/EAE range of the Alfvén spectrum in a tokamak plasma. These modes are potentially very important for tokamak reactor operation as they could render alpha particle orbits stochastic, degrading particle transport and confinement and modifying plasma heating profiles. Further experiments in ohmic and additionally heated

plasmas are expected to provide useful tests for the theories being developed to assess the stability of Alfvén eigenmodes in future ignition experiments.

The Authors would like to thank the JET Team for continued experimental support. This work was partly supported by the *Fonds national suisse pour la recherche scientifique* within a JET/CRPP Task Agreement.

References

[1] C.Z. Cheng, L.Chen and M.S.Chanse, *Ann. Phys.* (New York) **161**, 21 (1985).

[2] R.Betti, J.P.Freidberg, *Phys. Fluids B* **3**, 1865 (1991).

[3] G.Y.Fu and J.W.Van Dam, *Phys. Fluids B* **1**, 2404 (1989).

[4] D.J.Sigmar, C.T.Hsu, R.White and CZ.Cheng, *Phys. Fluids B* **4**, 1506 (1992).

[5] H.H.Duong et al., *Nucl. Fusion* **33**, 749 (1993).

[6] A.D.Turnbull et al., *Phys. Fluids B* **5**, 2546 (1993).

[7] K.L.Wong et al., *Phys. Rev. Lett.* **66**, 1874 (1991).

[8] W.W.Heidbrink et al., *Nucl. Fusion* **31**, 1635 (1991).

[9] S.Ali-Arshad and D.J.Campbell, to be published in *Plasma Phys. and Contr. Fusion.*

[10] W.W.Heidbrink et al., *Phys. Rev. Lett.* **71**, 855 (1993).

[11] E.Fredrickson et al., *Proc. of XV Int. Conf. on Plasma Phys. and Contr. Fusion, IAEA,* Seville, Spain (1994).

[12] A.Fasoli et al., submitted to *Phys. Rev. Lett.*.

[13] G.A.Collins et al., *Phys. Fluids B* **29**, 2260 (1986).

[14] G.A.Collins et al., *Plasma Phys. Contr. Fusion* **29**, 324 (1987).

[15] P.Descamps et al., *Phys. Lett.* A **143**, 313 (1990).

[16] R.R.Mett and S.M.Mahajan, *Phys. Fluids B* **4**, 2885 (1992).

[17] J.Candy and M.N.Rosenbluth, *Phys. of Plasmas* **1**, 356 (1994).

[18] H.L.Berk, R.R.Mett and D.M.Lindberg, *Phys. Fluids B* **5**, 3969 (1993).

[19] B.N.Breizman and S.E.Sharapov, submitted to *Plasma Phys. Contr. Fus.* (1995).

[20] G.M.Zaslavsky, et al., *Usp. Fiz. Nauk.* **156**, 193 (1988)

[21] A.Fasoli et al., *Phys. Rev. Lett.* **70**, 303 (1993).

[22] J.-M.Moret, *CRPP Laboratory Report* LRP 498/94 (1994).

[23] G.Huysmans et al., *Proc. XX Eur. Conf. on Controlled Fusion and Plasma Physics,* ed. by J.A.Costa Cabral, M.E.Manso, F.M.Serra, F.C.Schuller, EPS Lisbon, (1993) **I**, 187.

[24] L.Villard et al., *ibidem.*

[25] L.Villard and G.Fu, *Nucl. Fusion* **32**, 1695 (1992).

[26] S.Poedts et al., *Plasma Phys. Contr. Fusion* **34**, 1397 (1992).

[27] R.Betti, J.P.Freidberg, *Phys. Fluids B* **4**, 1465 (1992).

[28] N.N.Gorelenkov and S.Sharapov, *Physica Scipta* **45**, 163 (1992).

[29] J.Candy and M.N.Rosenbluth, *Plasma Phys. Contr. Fusion* **35**, 957 (1993).

[30] R.R.Mett and S.M.Mahajan, *Phys. Fluids B* **4**, 2885 (1992).

[31] E.J.Strait, W.W.Heidbrink and A.D.Turnbull, *Plasma Phys. Contr. Fusion* **36**, 1211 (1994).

[32] A.Jaun, Ph.D Thesis, *CRPP/EPFL Laboratory Report* LRP 513/95 (1995).

[33] G.T.A.Huysmans, J.P.Goedbloed and W.Kerner, *Phys. Fluids B* **5**, 1545 (1993).

[34] S.Brunner and J.Vaclavik, *Phys. Fluids B* **5**, 1695 (1993).

[35] J.W.Connor et al., *Proceeding of XXI EPS Conf. on Contr. Fus. Plasma Phys.*, **v. 18B** Part III, p.616 (1994).

[36] S.Sharapov et al., *Bull. Amer. Phys. Soc.* **39**, 1566 (1994) and *JET Report* JET-P(94) **61**, p.105 (1994).

Figure captions

Fig. 1 Experimental lay-out of the AE exciter and detection system.

Fig. 2 Example of a TAE resonance in the ohmic phase of JET shot #31638. Real and imaginary parts (left) and complex plane representation (right) of a magnetic probe signal, normalised to the driving current. The fit with B and A of order 5 and 2 is also shown, giving f_{obs}=144.2 +-0.1 kHz, $\gamma/2\pi$=1400 +-100 s^{-1}. $B_{tor} \cong 2.8$ T, $I_p \cong 2.2$ MA, $\bar{n}_e \cong 3x10^{19}$ m^{-3}; two upper saddle coils were used, in phase and 180^0 apart toroidally.

Fig. 3 Variation of the measured eigenmode frequency with toroidal magnetic field in JET shot #31591. B_{tor} varied linearly with time between 2.2 and 3 T; density and plasma current were kept constant; same saddle coils as in Fig. 1, but with opposite phase.

Fig. 4 Toroidal and poloidal mode structure of a TAE, represented as magnitude (+) and phase (x) of the residues fitted to the poloidal field pick-up coil signals, normalised to the saddle coil current. The driven spectrum, |n|=2, and the plasma parameters were as in Fig. 1. The poloidal angle is measured from the tokamak outer mid-plane upwards. The toroidal extension of the JET saddle coils is indicated as a shaded region. The poloidal angle for the toroidal array (top) is ~47^0, whilst the toroidal angle for the poloidal array (bottom) is ~17^0.

Fig. 5 Example of EAE observation. The driven response of a magnetic probe is shown as a function of the frequency for several successive scans along with the calculated $f_{EAE}^0 = 2f_{TAE}^0$. $\bar{n}_e \cong 4 - 8\ x10^{19}$ m^{-3}; $B_{tor} \cong 2.85$ T, $I_p \cong 2$ MA; |n|=2.

Fig. 6 The relationship between the profile of $g(r)=1/(q(r)\rho(r)^{1/2})$ and the TAE damping. g(r) and the raw and fitted frequency responses of a normalised magnetic probe signal are shown for two discharges. Excitation peaked at was used for both discharges; measurements were taken in the ohmic phase with similar plasma configuration; $\bar{n}_e \cong 4x10^{19}$ m^{-3}; (a) $B_{tor} \cong 1.8$ T, $I_p \cong 2$ MA. (b) $B_{tor} \cong 2.8$ T, $I_p \cong 2.3$ MA.

Fig. 7 B_{pol} probe signals for moderate (top) and high plasma current (bottom) in the same discharge #34073. Top: t = 3.5 s; $I_p \sim 2$ MA; $B_{tor} \sim 2.5$ T; $\langle n_e \rangle \sim 1.9\ 10^{19}$ m^{-3}; $T_e \sim 2.2$ keV. The single TAE has $f \approx 210.5$ kHz, $\gamma/\omega \approx 1.4$ %; $f_{TAE}^0 \sim 200$ kHz. Later, at t=9.5 s (bottom) a multiple peak structure appears, with $\Delta f/f \sim 2$ %; $I_p \sim 4.1$ MA; $B_{tor} \sim 2.9$ T; $\langle n_e \rangle \sim 3\ 10^{19}$ m^{-3}; $T_e \sim 3.2$ keV; $f_{TAE}^0 \sim 180$ kHz.

Fig. 8 Spectrum of magnetic (a) and density (b) perturbations in the Alfvén frequency range for a plasma heated by combined LHH (2.5 MW) and ICRH (6 MW), in an electron heating scheme (shot # 33157). The reflectometer frequency corresponds to the radial location r/a ~

0.5. Two successive scans, at t_1 = 19 s and t_2 = 20 s are shown. $I_p \sim 3$ MA; $B_{tor} \sim 3.2$ T; $\langle n_e \rangle \sim 2.5\ 10^{19}$ m^{-3}; $T_e \sim 6.3$ keV; $T_i \sim 2.9$ keV. $\Delta f/f \sim 2.5$ % and $\gamma/\omega < 10^{-3}$; $f_{TAE}^{\ 0}$ is indicated by the shaded region on the graph.

Fig. 9 Passive measurements: multiple peaks with ICRH heating producing resonant fast particles and low power NBI. Shot # 34188, t~15 s. ICRH: electron heating scheme (hydrogen minority resonance), P~7MW; NBI: P(80 kV)= 1.4 MW, P(140 kV)=1.6 MW; $I_p \sim 2.8$ MA; $B_{tor} \sim 3.1$ T; $\langle n_e \rangle \sim 2.5\ 10^{19}$ m^{-3}; $T_e \sim 7$ keV; $T_i \sim 5$ keV; $f_{TAE}^{\ 0} \sim 200$ kHz.

Fig. 10 Example of frequency distribution of the multiple kinetic AE driven by an external antenna for a number of additionally heated JET discharges.

Fig. 11 Alfvén spectrum for the equilibrium reconstructed for shot #33157 at t = 19 s. (a): continuous spectrum (CASTOR code). (b): detail of the most central minimum in the continuous spectrum above a TAE gap. The KTAE eigenfrequencies calculated by the CASTOR code using complex resistivity are indicated within the parabolic continuous spectrum profile and are shown in (c) as a function of the radial mode number. Bottom: calculated antenna-driven spectra, from CASTOR (d), corresponding to the eigenfrequencies reported in (b) and (c), and PENN (e) codes.

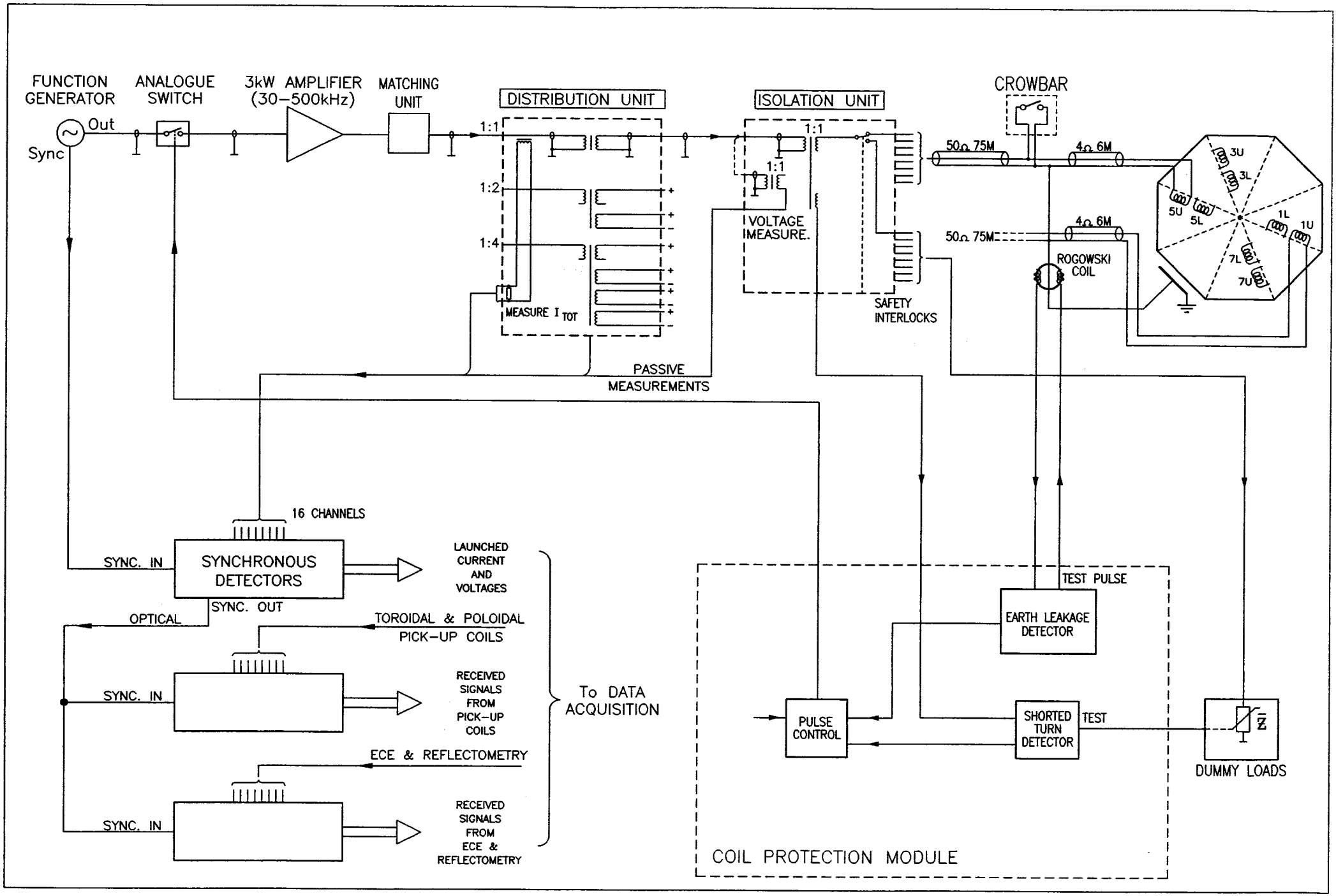

H:\VARIOUS\TAE5DIAG Tue May 16 13:56:53 1995

Fig. 1

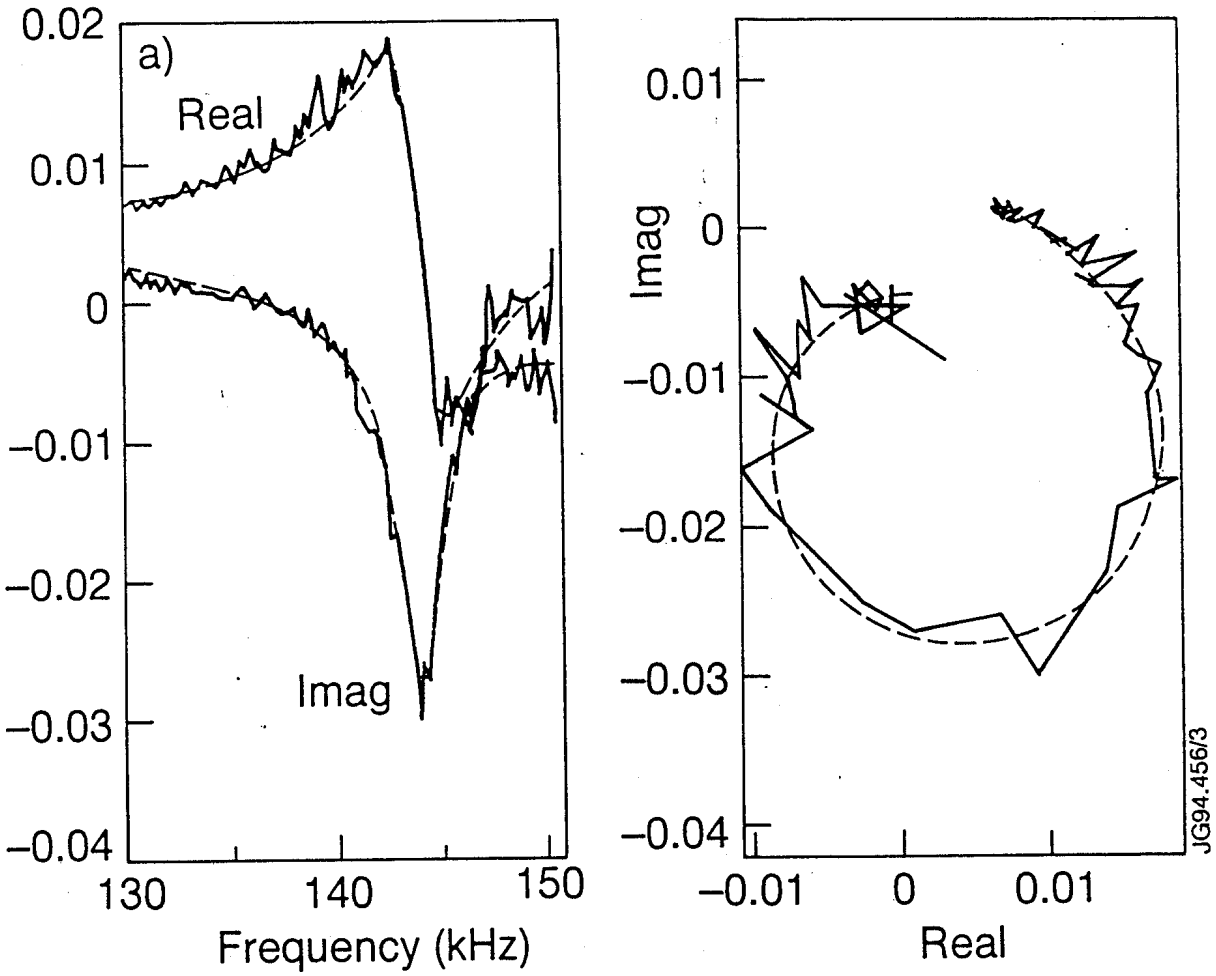
a)
Real
Imag
0.02
0.01
0
−0.01
−0.02
−0.03
−0.04
130
140
150
Frequency (kHz)
Imag
Real
JG94.456/3

Fig. 2

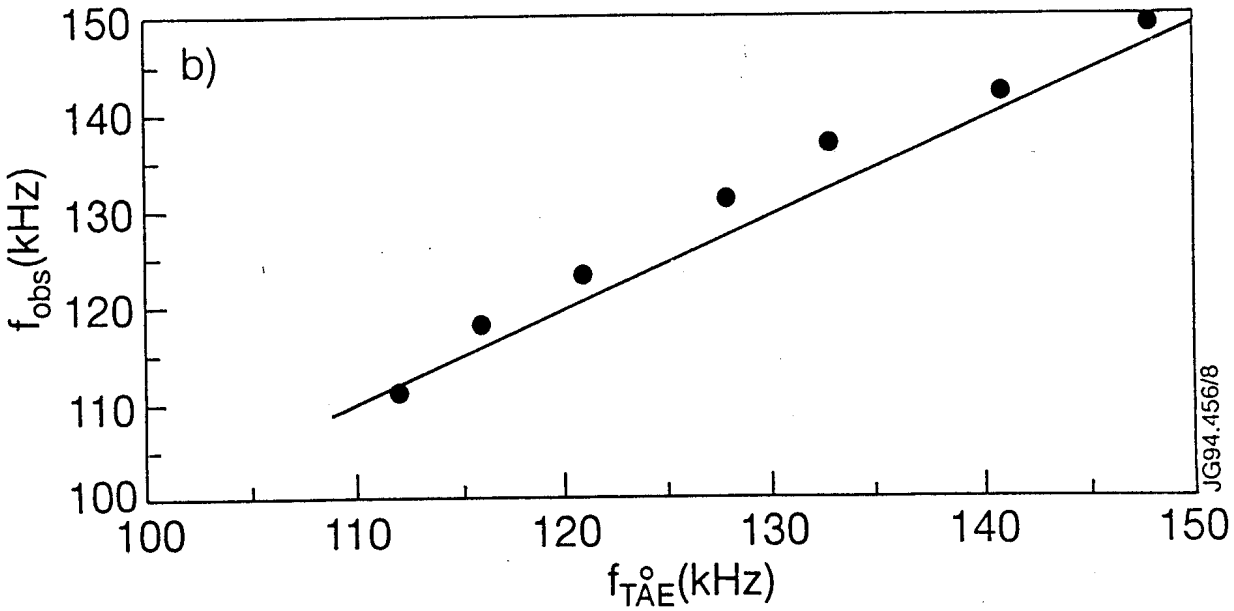
b)
150
140
130
120
110
100
100
110
120
130
140
150
f_{obs}(kHz)
f_{TAE}°(kHz)
JG94.456/8

Fig. 3

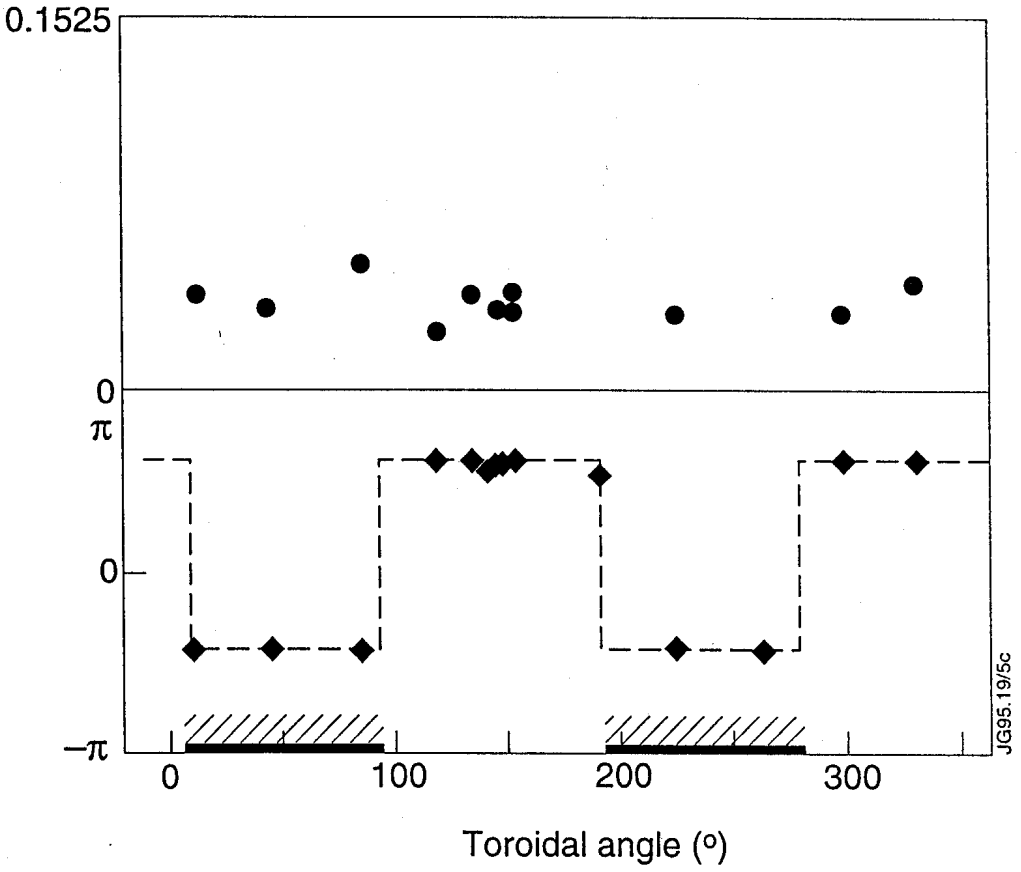
0.1525
0
π
0
−π
0
100
200
300
Toroidal angle (°)
JG95.19/5c

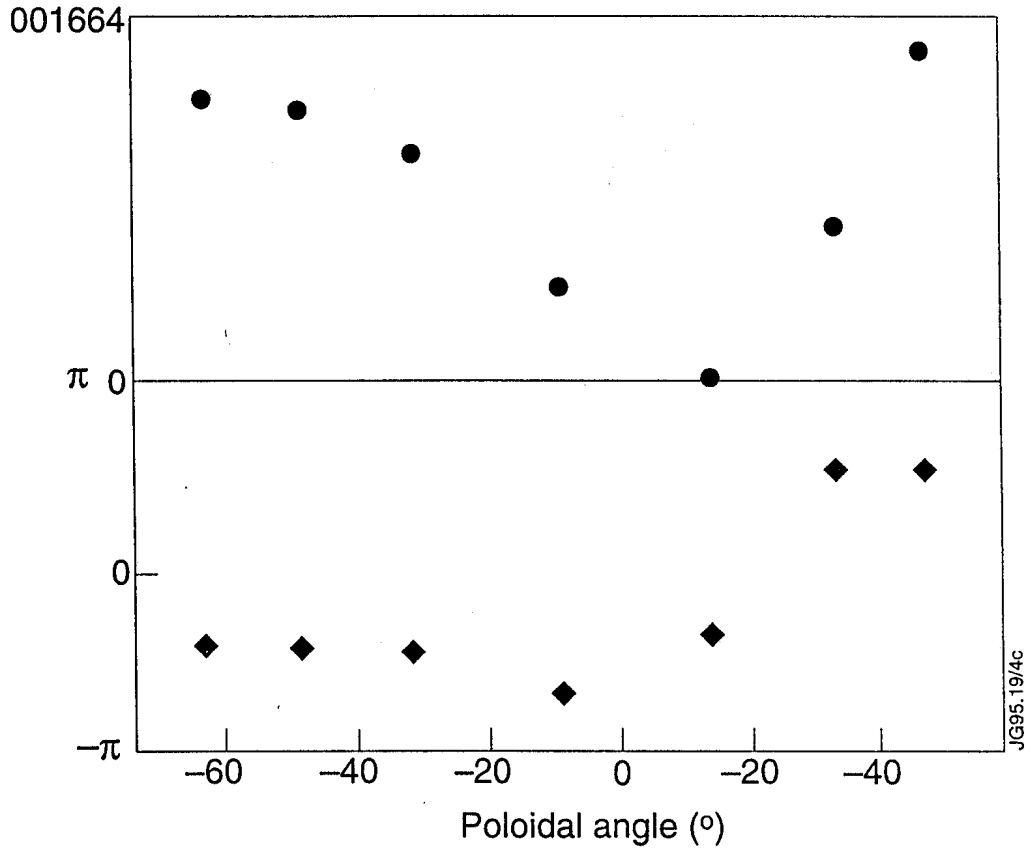
001664
π
0
0
−π
−60
−40
−20
0
−20
−40
Poloidal angle (°)
JG95.19/4c

Fig. 4

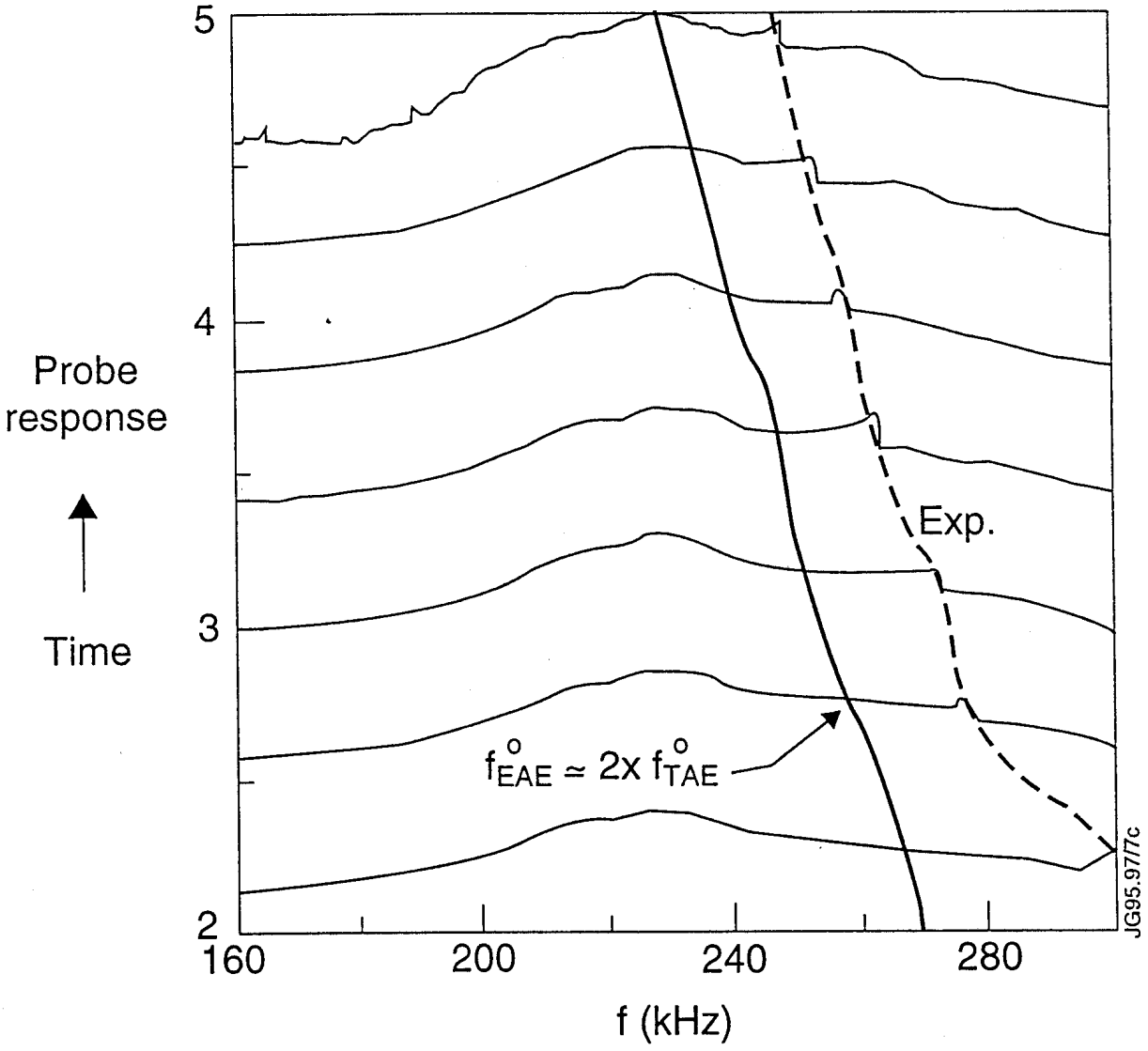
5
4
3
2
Probe
response
Time
Exp.
$f^{o}_{EAE} \simeq 2x\, f^{o}_{TAE}$
160
200
240
280
f (kHz)
JG95.97/7c

Fig. 5

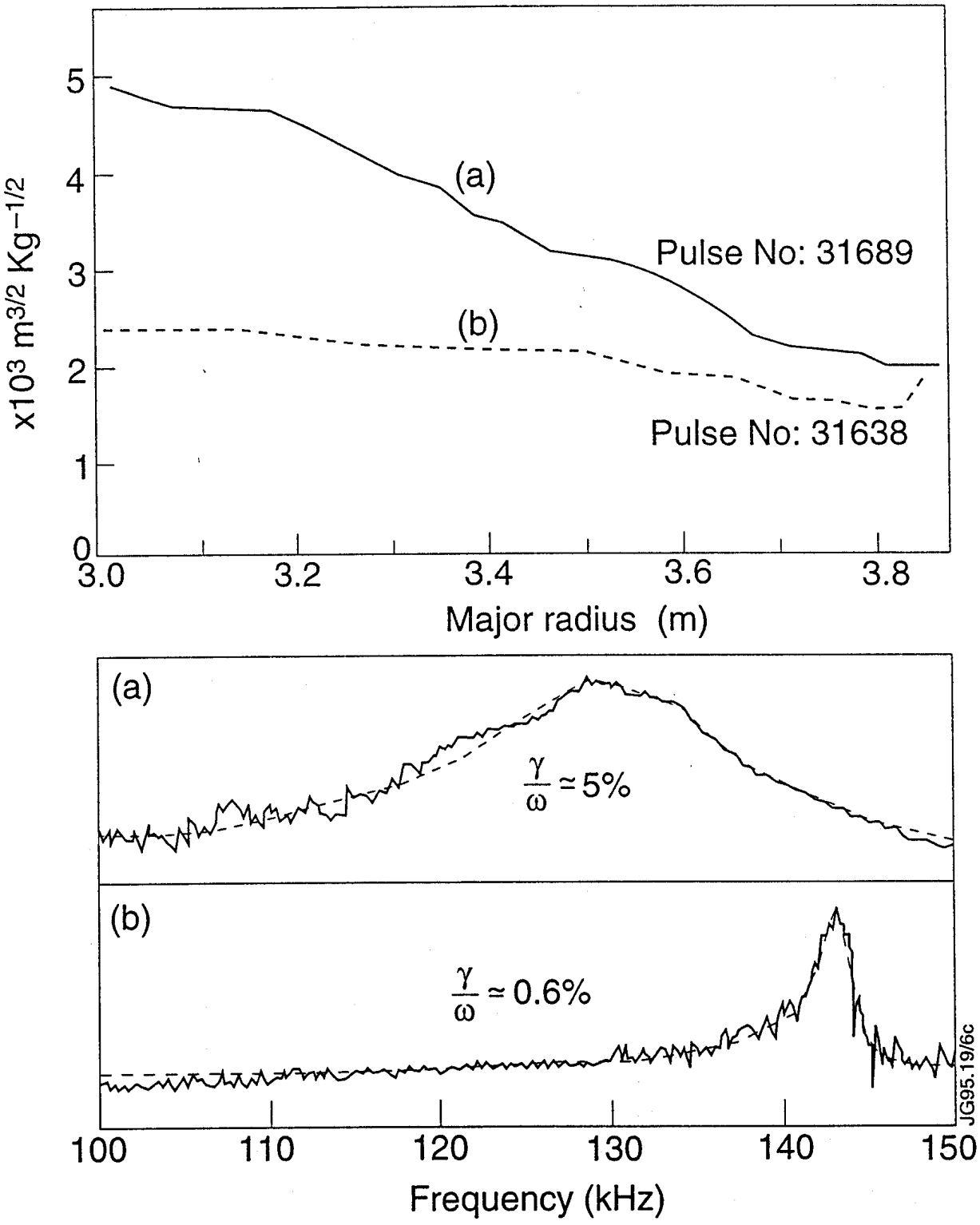
x10³ m³/² Kg⁻¹/²
5
4
3
2
1
0
(a)
Pulse No: 31689
(b)
Pulse No: 31638
3.0
3.2
3.4
3.6
3.8
Major radius (m)
(a)
γ/ω ≃ 5%
(b)
γ/ω ≃ 0.6%
100
110
120
130
140
150
Frequency (kHz)
JG95.19/6c

Fig. 6

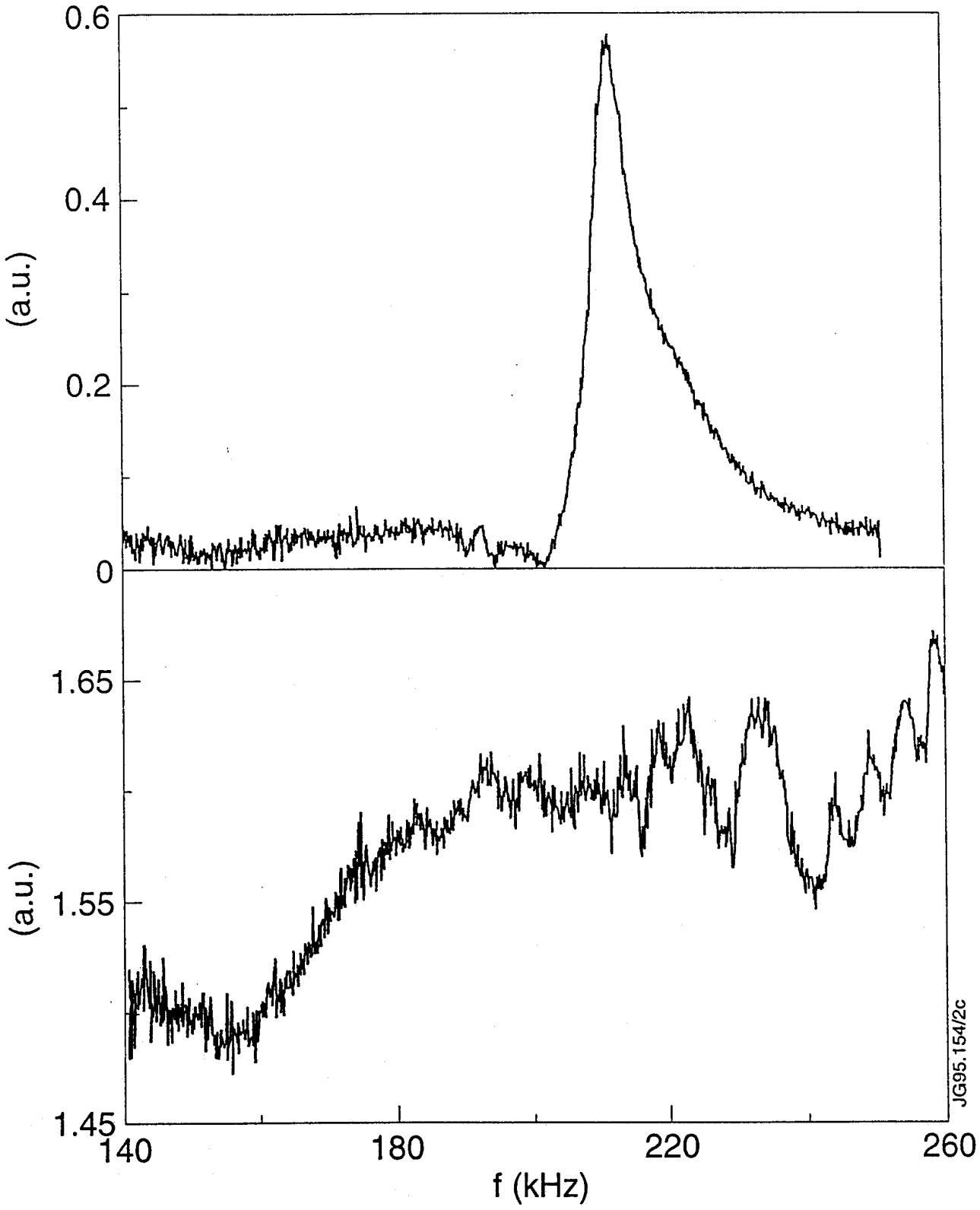

Fig. 7

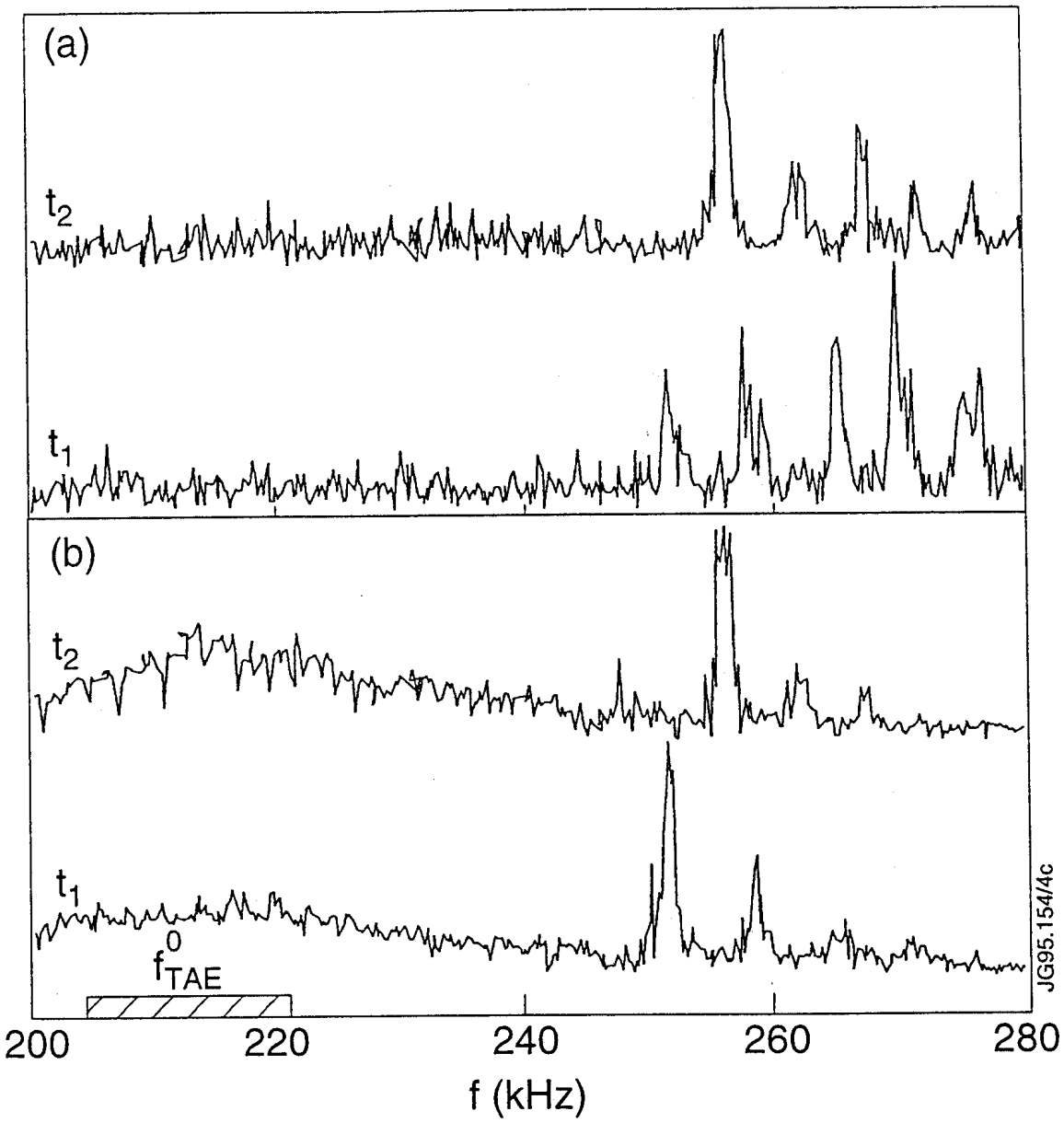

Fig. 8

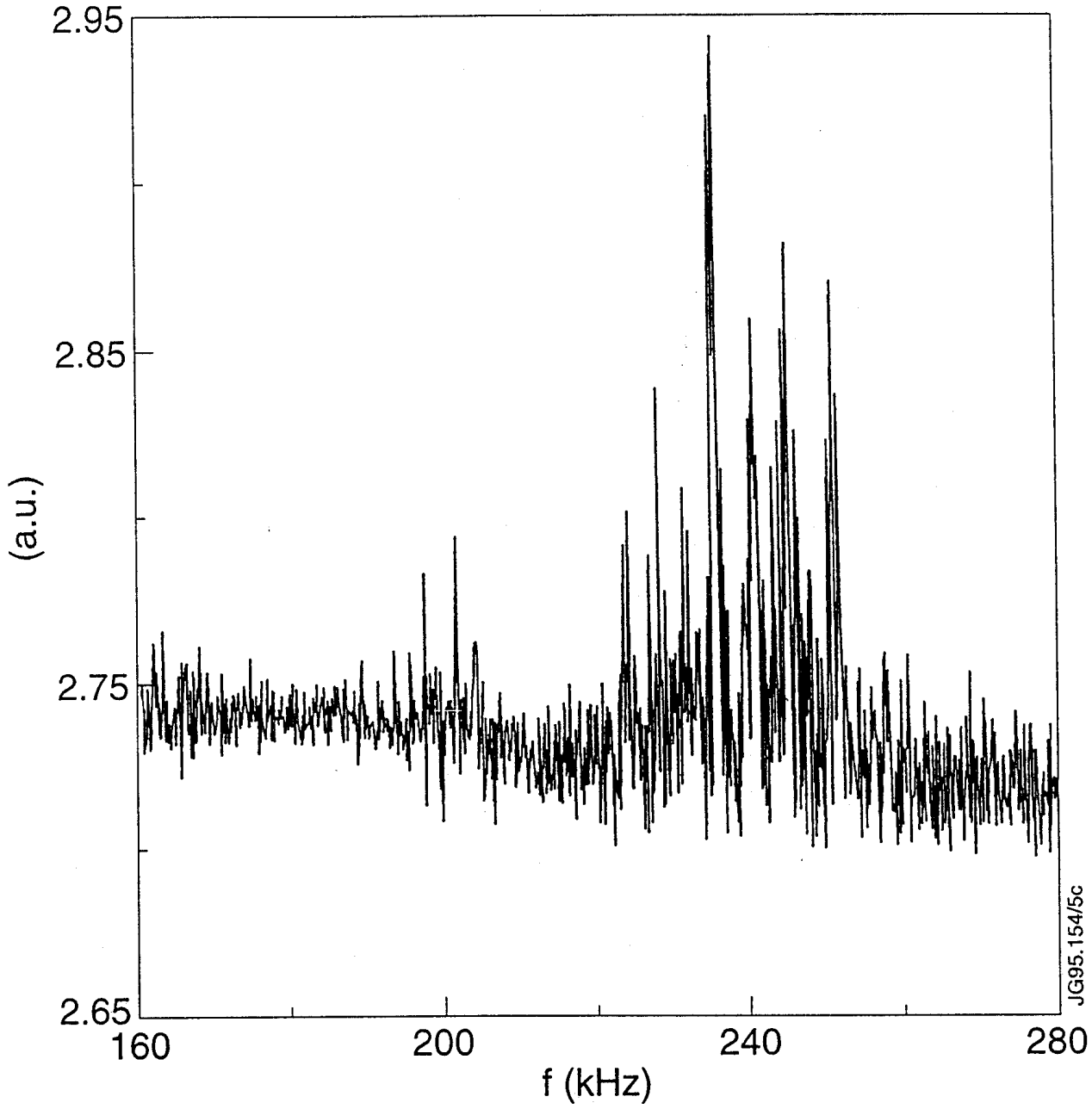

Fig. 9

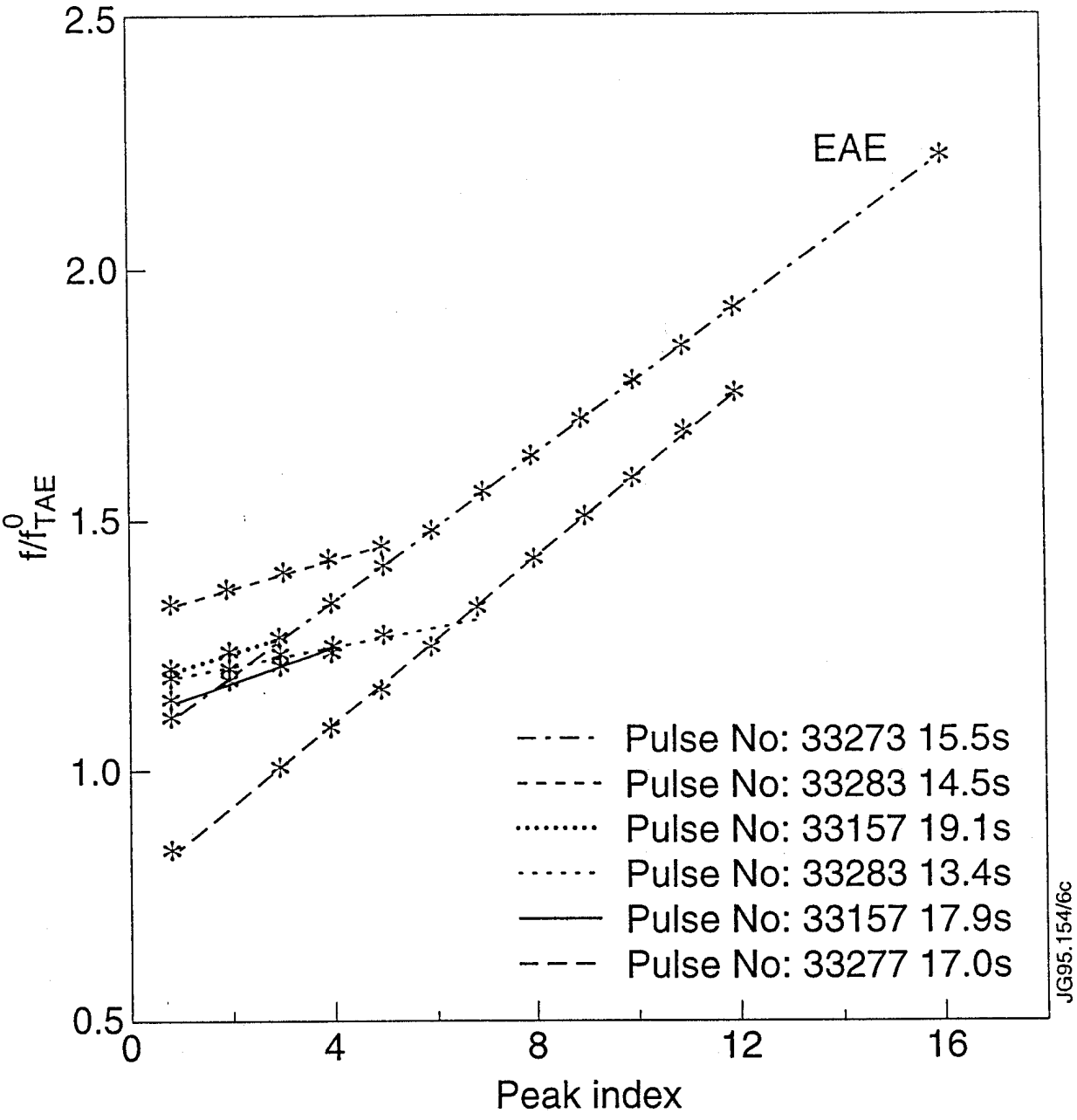
2.5
2.0
1.5
1.0
0.5
0
4
8
12
16
Peak index
f/f^0_{TAE}
EAE
Pulse No: 33273 15.5s
Pulse No: 33283 14.5s
Pulse No: 33157 19.1s
Pulse No: 33283 13.4s
Pulse No: 33157 17.9s
Pulse No: 33277 17.0s
JG95.154/6c

Fig. 10

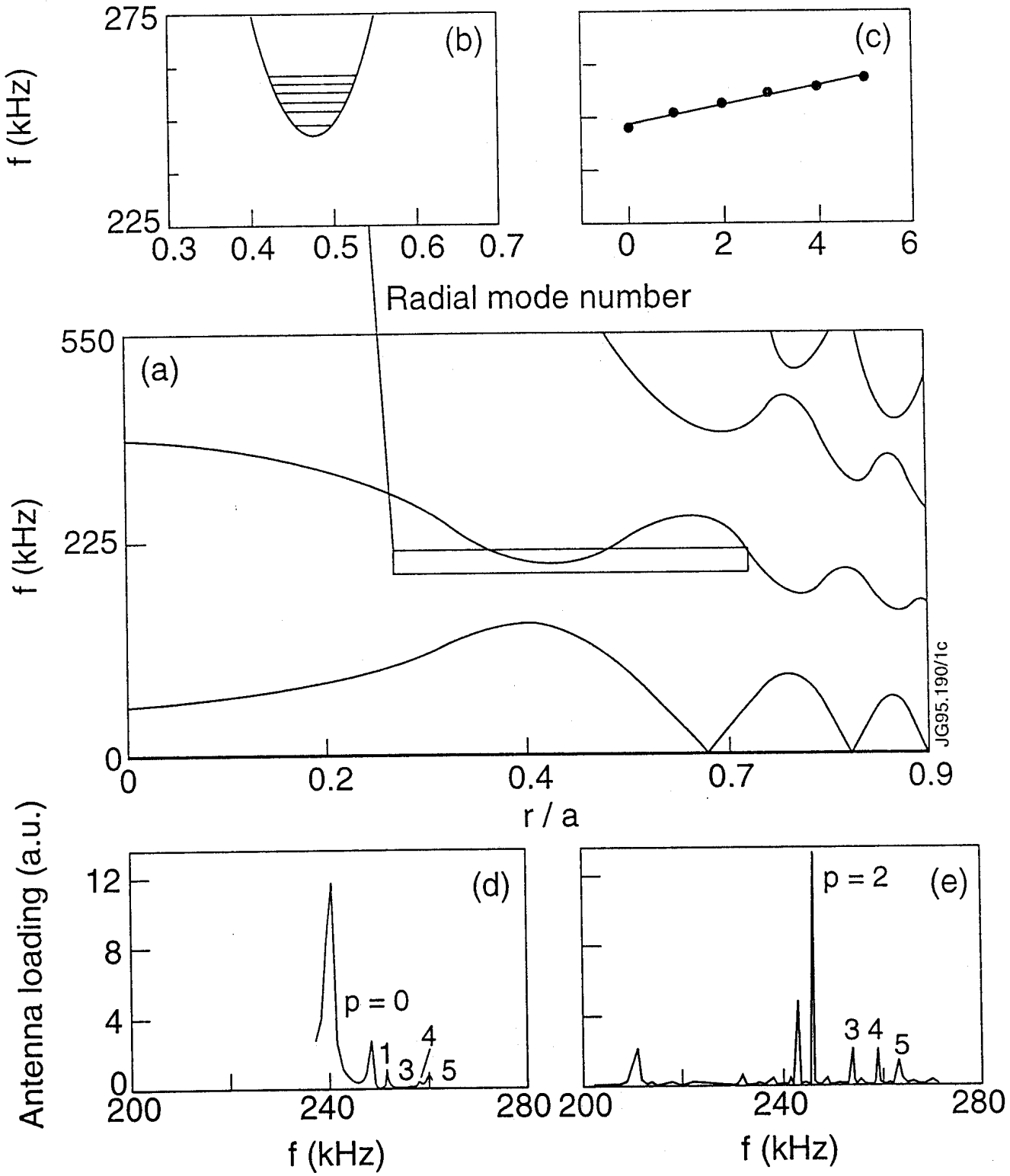
275
225
f (kHz)
(b)
0.3
0.4
0.5
0.6
0.7
(c)
0
2
4
6
Radial mode number
550
225
0
(a)
f (kHz)
0
0.2
0.4
0.7
0.9
r / a
JG95.190/1c
Antenna loading (a.u.)
12
8
4
0
(d)
p = 0
1
3
4
5
200
240
280
f (kHz)
p = 2
(e)
3 4
5
200
240
280
f (kHz)

Fig. 11